ABSTRACT

Waveform and Circuit Optimizations to Provide Spectral Compliance for Cognitive Radar

Matthew Fellows, M.S.E.C.E.

Mentor: Charles P. Baylis II, Ph.D.

Spectrum requirements on radar systems are becoming stricter due to the increasing number of wireless devices inhabiting the frequency spectrum. Future radar systems that are cognitive and flexible will be able to operate more effectively in the next-generation spectral environment. *Cognitive Radar* is a radar that can adapt to changing requirements placed upon it. The goal of the research presented in this thesis is to empower cognitive radar systems to adapt to changing requirements while maintaining the best level of performance possible. Maintaining that level of performance requires two things: adapting the radar waveform for optimum target detection capability and adapting the load impedance for optimum power efficiency while keeping in compliance with the spectrum requirements.

Waveform and Circuit Optimizations to Provide Spectral Compliance for Cognitive Radar

by

Matthew Fellows, B.S.E.C.E.

A Thesis

Approved by the Department of Electrical and Computer Engineering

_____

Kwang Y. Lee, Ph.D., Chairperson

Submitted to the Graduate Faculty of
Baylor University in Partial Fulfillment of the
Requirements for the Degree
of

Master of Science in Electrical and Computer Engineering

Approved by the Thesis Committee

_____

Charles P. Baylis II, Ph.D., Chairperson

_____

Robert J. Marks II., Ph.D.

_____

Truell Hyde II, Ph.D.

Accepted by the Graduate School

May 2014

_____

J. Larry Lyon, Ph.D., Dean

Page bearing signatures is kept on file in the Graduate School.

TABLE OF CONTENTS

LIST OF FIGURES

LIST OF TABLES

ACKNOWLEDGEMENTS

I would like to thank my advisor, Dr. Charles Baylis, for his continuing input and encouragement in both academic and personal pursuits. Dr. Robert Marks for his contributions to this work and to our entertainment. Larry Cohen of Naval Research Laboratory for his endless supply of ideas, field expertise, and connections. Previous students Matthew Moldovan, Josh Martin, and David Moon for their work getting this research going. Brandon Herrera for his assistance with the oscilloscope and other RF equipment. Pat Hynan for his tech support. I want to acknowledge Agilent Technologies for their cost-free loan of the Advanced Design System Software, Modelithics for their donation of simulation model libraries, and Maury Microwave for their donation of SNP customization files. I would also like to acknowledge the National Science Foundation and the Naval Research Laboratory for their funding of this work.

And I would like to thank my family members, Walt, Brenda, Sarah, and Samantha Fellows. Without all of you I would never have become who I am today.

CHAPTER ONE

Introduction

Power amplifiers for radar transmission are being placed under increasingly strict spectral requirements. The increasing number of wireless devices is forcing the devices already using the frequency spectrum to become smarter in order to perform their tasks without interfering with neighbors. This need for spectral sharing is especially shown by the National Broadband Plan of 2010. One provision in the Broadband Plan requires 500 MHz of currently occupied frequency space to be released over 10 years (by 2020). Much of that space will need to be taken from radar applications, forcing those radars to perform the same tasks with less spectrum. Reduced spectrum access is a particularly challenging problem for radar, since higher signal bandwidth often gives desirable detection characteristics for radar systems. So while compliance with new, stricter regulation is very important for radar systems, it is also important for the radar to get as much power and bandwidth out of the space available for it to use.

Radar's answer to the growing spectrum access problem is *cognitive radar*, which is envisioned as a type of radar system that will be able to adjust its operating characteristics to meet new requirements [38]. This would be especially useful in a potential dynamic spectrum access environment, which is a path the regulation may take to allow certain frequency bands to be shared between multiple users. In order for cognitive radar systems to become reality, algorithms will be needed for optimizing the various components of the new radar system.

This thesis presents two useful optimizations for cognitive radar. Chapter 2 includes the necessary background of important concepts involved in each search, as well as an establishment of the state of the art in related areas. In Chapter 3, an optimization is presented that will find the ideal load impedance for a radar power amplifier using a steepest-ascent, gradient-based search technique. The information in Chapter 3 was originally published in [1]. Chapter 4 presents an optimization which uses the radar ambiguity function to choose a good waveform for detection in the radar system. The information in chapter 4 was originally published in [2].

CHAPTER TWO

Background

In order to best understand the following chapters in this thesis, some background information about the subject matter is helpful. This chapter provides that background information and overviews the state-of-the-art in related work. Specifically, Section 2.1.1 will discuss information related to the presented load-pull circuit optimization, Section 2.1.2 will show the state-of-the-art in that area, Section 2.2.1 will discuss information related to the presented waveform optimization, and Section 2.2.2 will show the state-of-the-art in that area.

2.1 Background of Load-pull Circuit Optimization

2.1.1 Discussion of Key Concepts

The load-pull circuit optimization serves to make sure the amplifier load impedance used in a cognitive radar system is ideally chosen for two criteria: power-added efficiency (PAE) and adjacent channel power ratio (ACPR). PAE is a measure of how much of the DC power input to a power amplifier is converted to radio frequency (RF) power output from that amplifier. PAE is defined by

$$PAE = \frac{P_{out,RF} - P_{in,RF}}{P_{DC}} \times 100\%. \tag{2.1}$$

Ideally PAE should be as high as possible for a power amplifier.

ACPR measures the ratio of the power that spreads into neighboring bandwidths to the power in the main operating frequency band used by an amplifier. ACPR should be

a small number, since larger amounts of power in adjacent channels will be more likely to interfere with other devices attempting to use those frequency bands. Power from the amplifier leaks into the adjacent channels due to nonlinearities in the amplifier that result in spreading out the frequency spectrum output from the amplifier [13]. In the United States, this spectral spreading for radar is governed by the Radar Spectrum Engineering Criteria (RSEC), which are created by the National Telecommunications and Information Administration (NTIA) in the United States. The regulation for spectrum use takes the form of a spectral mask, which is simply a line that the measured spectrum cannot go above. Compliance with the spectrum regulations in the load-pull circuit optimization is achieved by setting a limit value of ACPR that is not exceeded by the chosen operating condition at the end of the optimization. An example of a spectral mask is shown in Figure 2.1.

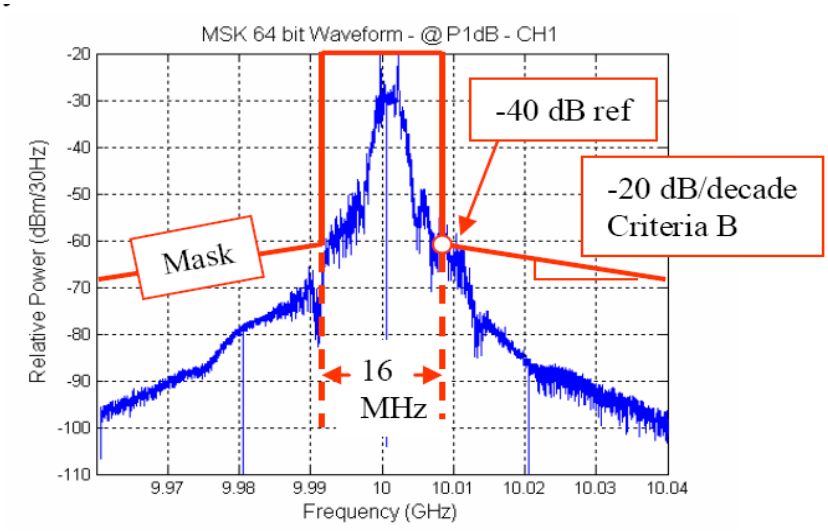

Figure 2.1 Example Spectral Mask (reprinted from [3])

PAE and ACPR are both functions of the load reflection coefficient Γ_L of the amplifier [12]. Those functions are best shown using contours on a Smith Chart as shown in Figure 2.2. Each point on one of those contours will have the same value for the related function, with the values for PAE getting smaller as the contours recede from the PAE maximum, and the values for ACPR getting bigger as the contours recede from the ACPR minimum. Note that the Smith Chart contours are specific to the device being tested, so the set shown in Figure 2.2 is only for one device. For a balance between PAE and ACPR, the ideal operating Γ_L can be defined as the value of Γ_L which gives the highest PAE within an ACPR limit, thus giving good efficiency while assuring spectral compliance. If one varies the ACPR limit and finds the best PAE measurement for all possible ACPR limits, the results will form a line of points connecting the PAE maximum to the ACPR minimum on the Smith Chart. This line is called the *Pareto Front* [4, 5].

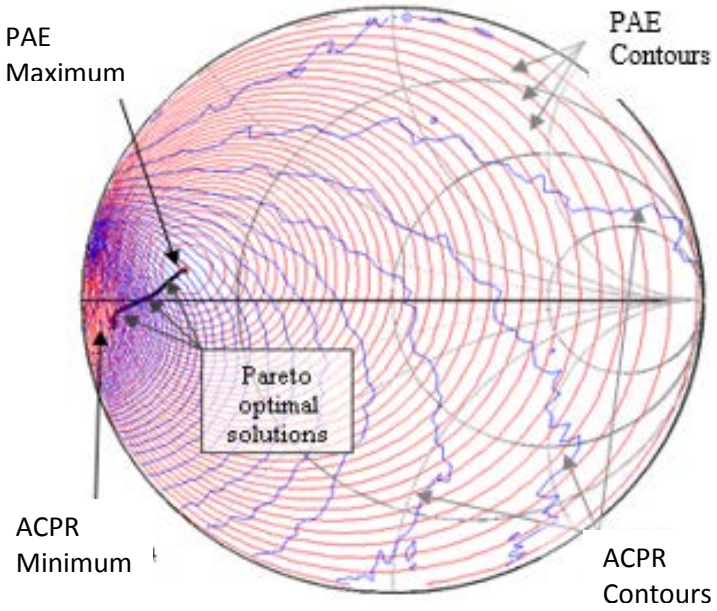

Figure 2.2 Example Contour Plots for PAE and ACPR. The PAE maximum and the ACPR minimum are indicated, as is the Pareto Front connecting the two.

[4] presented the first version of an algorithm designed to find the best PAE within an ACPR limit for an amplifier. That optimization worked by starting from an arbitrary location on the Smith Chart and proceeding to the optimum Γ_L by taking the path of steepest ascent for PAE until the PAE maximum was reached, and then stepping down the Pareto Front until the search was under the ACPR limit. That algorithm achieved its goal, but the indirect path (going to the PAE maximum first) resulted in extra measurements being required to find the optimum. Chapter Three of this thesis presents a new optimization algorithm that takes a more direct path to the optimum Γ_L, which results in a significant savings in measurements required for the algorithm to complete.

2.1.2 State of the Art in Load-Pull Optimization

This subsection contains a brief overview of the literature references related to the presented work on circuit optimization. [5] describes basic principles of Pareto optimization. [6,7,8,9,10,11] are other papers involving Pareto optimization for a tradeoff between two objectives depending on common variables. PAE and ACPR's dependence on Γ_L is shown in [12]. [13] addresses amplifier distortion due to nonlinearity. [14] recommends ACPR as a significant indicator of out-of-band emissions. [15,16] include considerations of intermodulation between in-band frequency components, resulting in spectral spreading. [12,17] represent earlier work on ACPR load-pull and ACPR's dependence on load impedance.

[18] relates ACPR results for broadband signals to predictions based on intermodulation measurements. [19,20] demonstrate the use of a genetic algorithm for matching antenna impedance based on the voltage standing wave ratio. [21] shows that

real-time transmitter optimization is feasible using a genetic algorithm for tuning a transmitter amplifier with matching networks. [22] examines genetic algorithms and notes that they tend to be slower than other algorithms for some impedance-matching optimizations. [23,24,25] propose other matching network optimization approaches including fuzzy control [23], neural networks [24], and least-squares optimization [25]. [26] is a paper from 2011 work at Baylor Wireless and Microwave Circuits and Systems (WMCS) demonstrating a steepest-ascent algorithm for one-objective impedance optimization – optimizing output power. Baylor WMCS also created [27], which demonstrates the dependence of PAE and ACPR on amplifier load impedance for LFM chirp waveforms.

2.2 Background of Waveform Optimization

2.2.1 Discussion of Key Concepts

The waveform optimization works to make sure that the waveform chosen by a cognitive radar system is ideal for target detection. This is performed through use of the ambiguity function, which is defined as

$$\chi(\tau, u) = \int_{t=-\infty}^{\infty} s(t)\, s^*(t-\tau) e^{-j2\pi u t} dt. \tag{2.2}$$

$s(t)$ is the transmitted radar signal, τ is the difference in time from the actual time delay associated with a target, and u is the difference in Doppler frequency shift from the actual Doppler shift of a target. As explained in detail in Chapter 4, the integral represents a variation in the correlator's output over these differences in time and Doppler from the true time and Doppler of the target. The variation of the integral's value over these two differences will correspond with the transmitted signal's ability to

provide resolution in range and target speed. Thus the ambiguity function provides a measure of how well a radar waveform will detect range and speed characteristics of a target. The ideal ambiguity function for target detection would have a high value of the ambiguity function at the origin ($\tau = 0, u = 0$) and a zero value everywhere else. This would indicate that particular signal gives a high return at the target's actual range-Doppler coordinates and a low return elsewhere. However, no waveform exists that gives those zero values everywhere except the origin [32].

Magnitude plots of some example ambiguity functions are shown in Figures 2.3, 2.4, and 2.5. The result in Figure 2.3 is the ambiguity function for a time domain impulse function. This would be the ideal waveform for range detection of a target, as the ambiguity is aligned along the *u* axis. This also makes intuitive sense, as it would be very easy to calculate the time delay for an impulse function, but there would be no frequency shift information to use for finding speed.

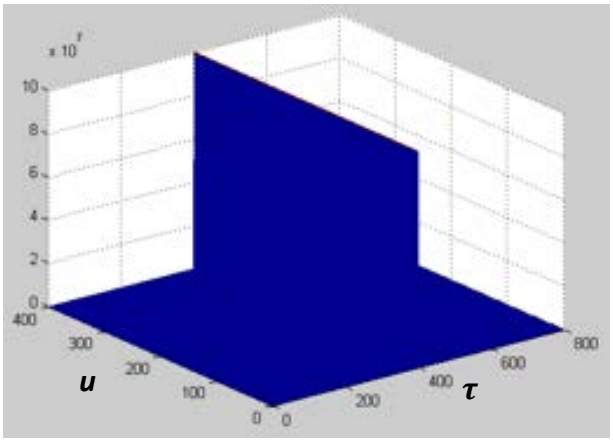

Figure 2.3 Ambiguity function magnitude for time domain impulse

Figure 2.4 shows the ambiguity function magnitude for a time domain sinusoid at constant frequency. A sinusoid is the intuitively ideal function for detecting speed, since one frequency gives very good Doppler detection capability. The high values in ambiguity in Figure 2.4 align along the τ axis, which fits with the intuition. There is some spreading out of the ambiguity in the figure, which is due to the time-limited nature of the sinusoid being used.

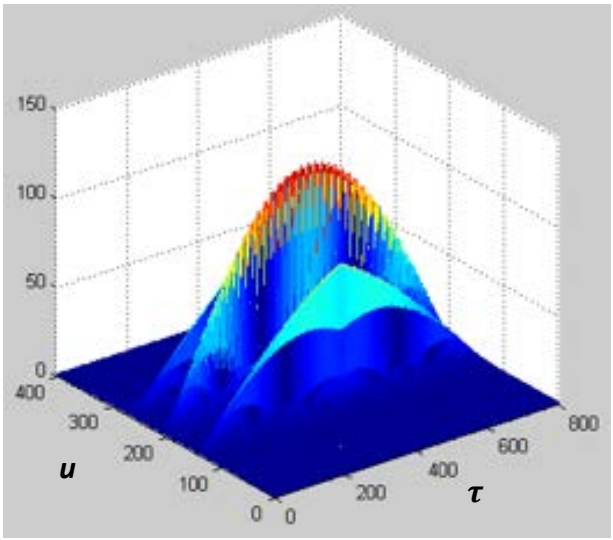

Figure 2.4 Ambiguity Function Magnitude for time domain sinusoid

Figure 2.5 shows the ambiguity function for a linear frequency-modulated (LFM) chirp. A chirp is simply a sinusoid that increases or decreases over the time duration of its pulse. The chirp waveform is unique as it creates a narrow triangular ridge in the ambiguity function, with a tilt angle based on the ratio to the bandwidth of the chirp to the time length of the pulse. LFM chirps are very commonly used radar waveforms, and the waveform optimization presented in chapter 4 adjusts the ambiguity function by

changing the bandwidth of the chirp in order to alter the tilt angle of the ridge in the ambiguity function.

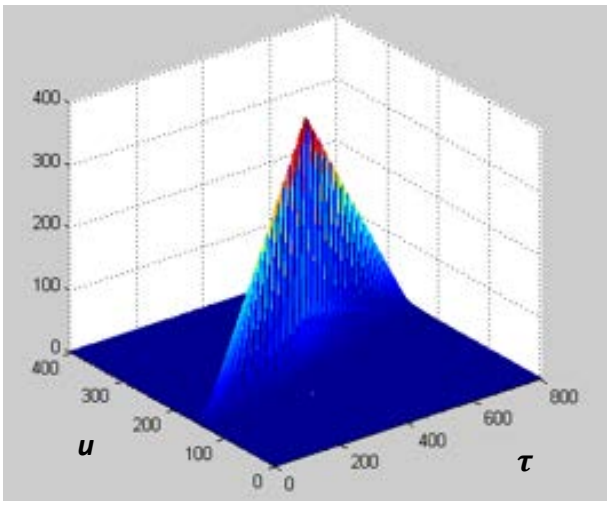

Figure 2.5 Ambiguity Function for LFM Chirp

2.2.2 State of the Art in Waveform Optimization

This subsection contains an overview of literature references related to the presented work on waveform optimization. [28,29,30,31] show design of spectrally confined waveforms through various techniques. [28] used variable-modulus techniques, [29,30] used constant-modulus continuous phase modulation to minimize spectral spreading of waveforms. [31] used constant-modulus piecewise chirp optimization. [32] discussed the connection of ambiguity function with the waveform, including characteristics of chirps. [33] demonstrates optimization of LFM chirp design by tuning the nonlinear Fourier Series perturbations to phase. [34] uses the ambiguity function surface as a weighted error criterion for waveform optimization. [35] uses genetic algorithms to minimize the ambiguity function volume in different regions of the range-Doppler plane. [36] applies least-squares optimization to radar waveforms.

2.3 Summary

This chapter has shown background information in the areas of load-pull optimization and waveform optimization. Related to the load-pull optimization, this chapter has discussed PAE, ACPR, their relation to load reflection coefficient Γ_L, and the Pareto Front of optimum solutions for different ACPR limits. Related to waveform optimizations, this chapter has described the ambiguity function and shown some ambiguity function results for simple waveforms. Chapter 3 and Chapter 4 will use the information from this chapter as a launching point for describing the presented optimizations.

CHAPTER THREE

Direct Radar Amplifier Load-pull Optimization

This chapter has been accepted for publication as: [1] Fellows, M.; Baylis, C.; Martin, J.; Cohen, L.; Marks, R.J., "Direct Algorithm for the Pareto Load-Pull Optimization of Power-Added Efficiency and Adjacent-Channel Power Ratio," –accepted for publication by IET Radar, Sonar, and Navigation

In order to improve upon the previously designed load-pull optimization described in [4], an algorithm was needed that would use fewer measurements to find the optimum load reflection coefficient Γ_L for a radar power amplifier. The new algorithm achieves that goal using a vector-based method to more directly approach the optimum instead of finding the PAE maximum first. Section 3.1 describes the new algorithm, Section 3.2 shows results for computer simulations of the algorithm, and Section 3.3 shows test bench measurement results for the direct load-pull algorithm.

3.1 Method for Direct Load-pull Optimization

The direct load-pull optimization is designed to start at an arbitrary reflection coefficient and take steps on the Smith Chart toward the optimum load impedance from there. As mentioned previously, the optimum reflection coefficient is defined as the location on the Smith Chart which contains the maximum PAE for a specified ACPR limit. At each candidate location three measurements on required. These measurements find the PAE and ACPR at the candidate point and at two neighboring points, which are separated from the candidate point by user-defined parameter D_n as shown in Figure 3.1 below.

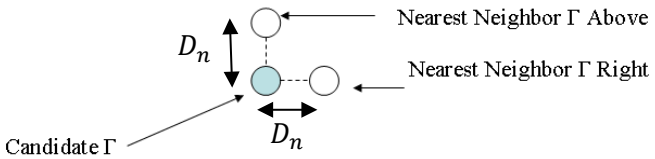

Figure 3.1: Measurements required at each candidate location

Using these measurements allows for gradients to be calculated for PAE and ACPR. That gradient is then used to find the directions of steepest ascent for PAE and steepest descent for ACPR. The algorithm then proceeds using equations 3.1-3.4:

$$\bar{v} = \hat{a}D_a + \hat{b}D_b \tag{3.1}$$

$$\bar{v} = \hat{p}D_a + \hat{b}D_b \tag{3.2}$$

$$D_a = \frac{D_s}{2}\frac{|ACPR_{meas} - ACPR_{target}\,|}{|ACPR_{worst} - ACPR_{target}|} \tag{3.3}$$

$$D_b = \frac{D_s}{2}\frac{|\theta_{meas} - \theta_{target}\,|}{\theta_{target}} \quad . \tag{3.4}$$

(3.1) and (3.2) describe the possible step vectors that can be used in the search. (3.3) and (3.4) describe the magnitude used for each component of those step vectors. In those formulas, $\hat{a}$ and $\hat{p}$ represent unit vectors in the directions of steepest descent for ACPR and steepest ascent for PAE respectively. $\hat{p}$ is the unit vector in the direction of the bisector angle between $\hat{a}$ and $\hat{p}$. D_a and D_b are the vector magnitudes that will be used with their associated vectors.. D_s is the user-defined parameter which determines the largest possible step size. The various ACPR and θ terms reference the appropriate ACPR value and bisector angle between the PAE and ACPR gradients, respectively. $ACPR_{worst}$ is the "worst" value of ACPR that has been measured by the search, where the worst value is chosen to be the value that maximizes $|ACPR_{worst} - ACPR_{target}\,|$. In

most cases, $ACPR_{worst}$ will be either the first measured ACPR or the measured ACPR at one of the first two neighboring points. However, the value is recalculated every time a new ACPR value is measured. $ACPR_{target}$ is the ACPR limit for the search. θ_{target} is equal to 90°, which is due to the fact that $\hat{a}$ and $\hat{p}$ will be pointing in opposite directions when the search is located on the Pareto Front. Thus a bisector angle of 90° indicates that the candidate point is on the Pareto Front, which is where D_b should equal zero.

Using these equations the search proceeds in one of two ways. If the ACPR measurement at the current candidate location is greater than the ACPR limit, the search uses (3.1) for the step vector. This indicates that the current candidate is not meeting spectral regulations and needs to improve in ACPR. If the ACPR measurement at the current candidate is less than the ACPR limit then the search uses (3.2) for the step vector. This indicates that the search is complying with spectral regulations and needs to improve in PAE. Figure 3.2(a) and Figure 3.2(b) show representations of these two step methods.

Once the search enters the spectrally compliant region of the Smith Chart, two final considerations are added to the process. After each step, the algorithm checks if the new candidate point is (1) out of ACPR compliance (above the ACPR limit) or (2) has a lower PAE than the previous candidate. In either case, the search returns to the previous location and divides the value of D_s by 3. These situations indicate that the algorithm stepped too far, overshooting the ACPR limit contour and/or the Pareto Front.

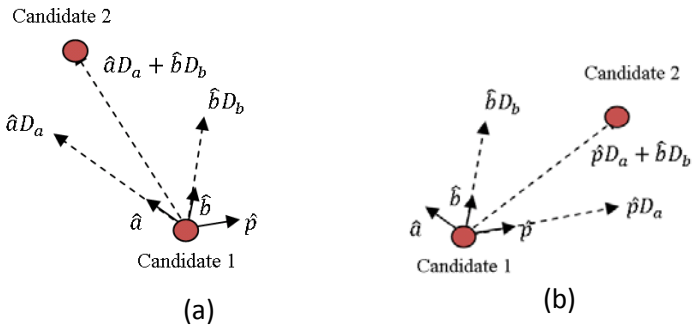

Figure 3.2: Representation of the step vector when (a) ACPR measured at Candidate 1 is greater than the limit (not spectrally compliant), or (b) ACPR measured at Candidate 1 is less than the limit (spectrally compliant)

Finally, the search terminates when the calculated vector step magnitude $|\bar{v}|$ is less than the neighboring-point distance D_n, which is a user-defined parameter. Once that condition is met, the measured Γ_L with the highest PAE within the ACPR limit is chosen as the optimum load reflection coefficient. This Γ_L is typically either the last measured candidate point or one of the neighboring points for the second to last candidate.

3.2 Computer Simulation Results using ADS

The first method used for validating the specified algorithm was to use Agilent Advanced Design System (ADS) with a nonlinear field-effect transistor (FET) model from Modelithics. The specific simulated device for the results in this section was a TriQuint TGF2960-SD Packaged HFET. The device was biased with $V_{DS} = 8$ V and $I_D = 10$ mA. The input signal for these simulations is a CDMA signal centered at 800MHz with an available power of 11dBm. These settings resulted in the load-pull contours shown in Figure 3.3 below. Note that the ACPR minimum, and PAE maximum, and Pareto optimum locations are all shown.

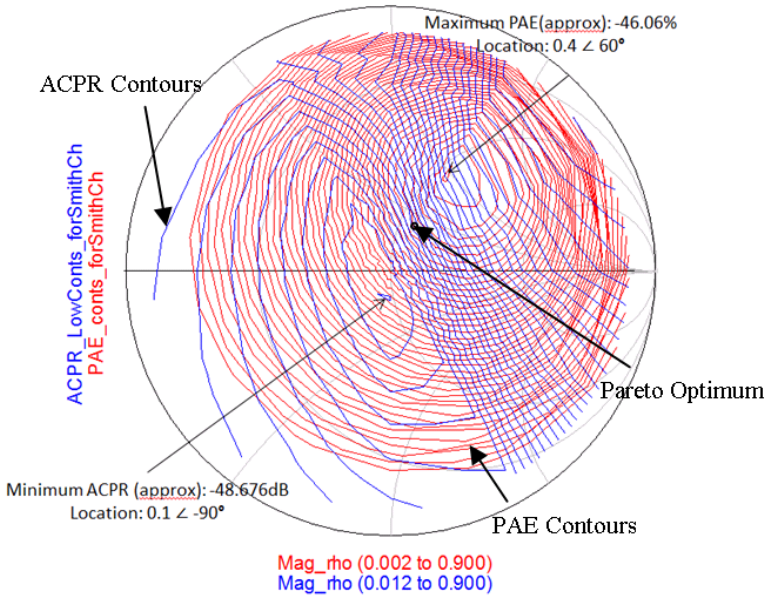

Figure 3.3: PAE and ACPR contours for simulated load-pull data

Figures 3.4-3.8 show the results for running the presented algorithm from several start locations on the Smith chart using an ACPR limit of -45 dBc. For each result the starting value of Γ_L, the end value of Γ_L, the final PAE, the final ACPR, and the number of measurements taken are shown in each figure. The results from these simulations are also compiled in Table 3.1.

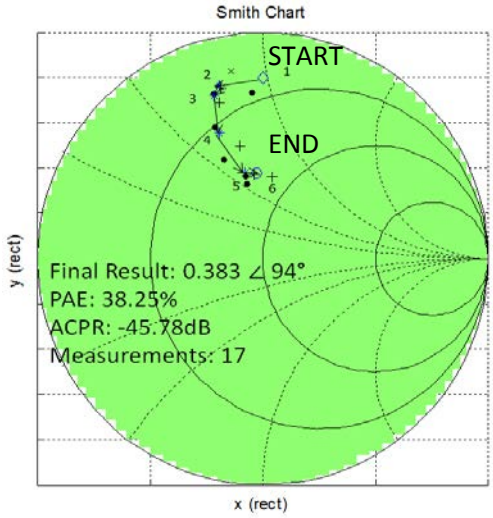

Figure 3.4: Simulated search result for start location Γ_L =0.8 ∠ 90°

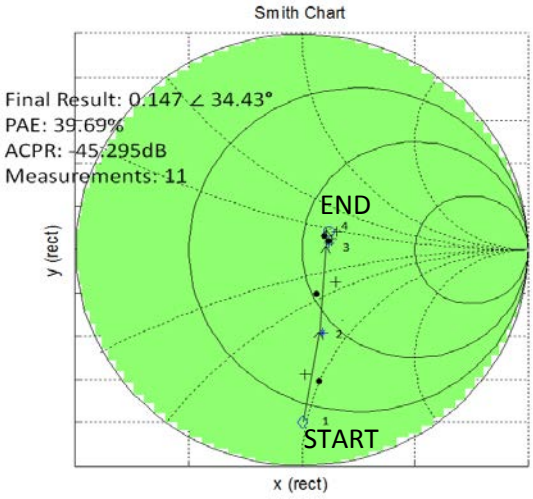

Figure 3.5: Simulated search result for start location Γ_L =0.8 ∠ -90°

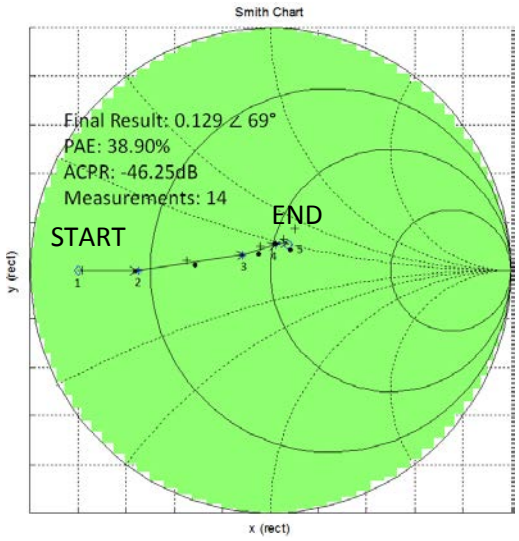

Figure 3.6: Simulated search result for start location $\Gamma_L = 0.8 \angle 180°$

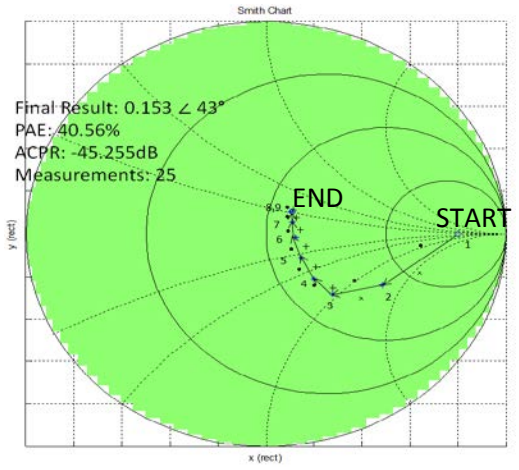

Figure 3.7: Simulated search result for start location $\Gamma_L = 0.8 \angle 0°$

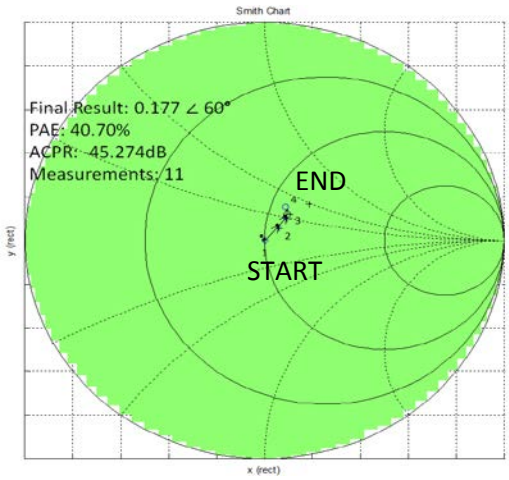

Figure 3.8: Simulated search result for start location $\Gamma_L = 0 \angle 0°$

Table 3.1: Simulation results for different starting reflection coefficients

Start Γ_L	**End Γ_L**	**End PAE (%)**	**End ACPR (dBc)**	**# Pts.**
0.8 <90º	0.383<94º	38.25	-45.78	17
0.8 <-90º	0.147<34º	39.69	-45.30	11
0.8 <180º	0.129<69º	38.90	-46.25	14
0.8<0º	0.153<43º	40.56	-45.26	25
0	0.177<60º	40.70	-45.27	11

As these results show, the algorithm consistently attains measured values of ACPR less than the limit of -45dBc and attains similar results for PAE from all start locations, which indicates that the algorithm is attaining acceptable results. Furthermore, the variation in number of measured points for this algorithm varies from 11 to 25 points, which is much less than the number of points required for similar searches using the method described in [4]. These results do show some variation in the search's end locations, but these variations are acceptable due to the closeness of the PAE results. These variations in location also make sense if the load-pull contours are examined, since the contours in the optimum region stretch from the top of the Smith chart toward the

bottom of the chart. So the simulation results show an acceptable level of performance for the presented algorithm.

3.3 Test Bench Results

Once the algorithm had been validated in computer simulations it was tested using the bench-top load-pull system at the Baylor Research and Innovation Collaborative. That system uses a Maury Microwave Automated Tuner System (ATS) being controlled by MATLAB through a GPIB connection. To vary the load impedance, the ATS system uses mechanical tuners to adjust the reflection coefficient at the load of the amplifier under test. The bench top setup also includes a signal generator to produce LFM chirp waveforms, a DC power supply for amplifier biasing, a power meter for PAE measurements, and a spectrum analyzer for ACPR measurements. Figure 3.9 shows a picture of the load-pull system, which is also described in more detail in [37].

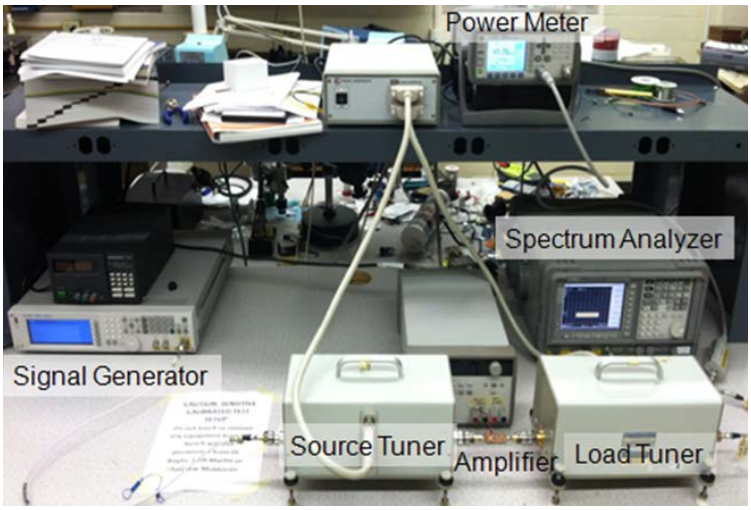

Figure 3.9: Load-pull test bench system

For the testing of the presented algorithm, a Skyworks SKY65017-70LF InGaP amplifier was used as the device under test. The bias conditions used a 9V DC power input with 100 mA of current. The input waveform was a LFM up chirp with 16 MHz bandwidth at a center frequency of 3.3 GHz and an input power of 2.0 dBm. In addition to testing the presented algorithm on the test bench, the algorithm from [4] was tested in order to provide a comparison. Figure 3.10(a) shows the load-pull contours for this device and Figure 3.10(b) shows the Pareto optimum found by a traditional load-pull. Figure 3.11(a) – Figure 3.11(j) show the results for running each algorithm from various start locations. The results for the new algorithm are summarized in Table 3.2, and the results from both algorithms are compared in Table 3.3.

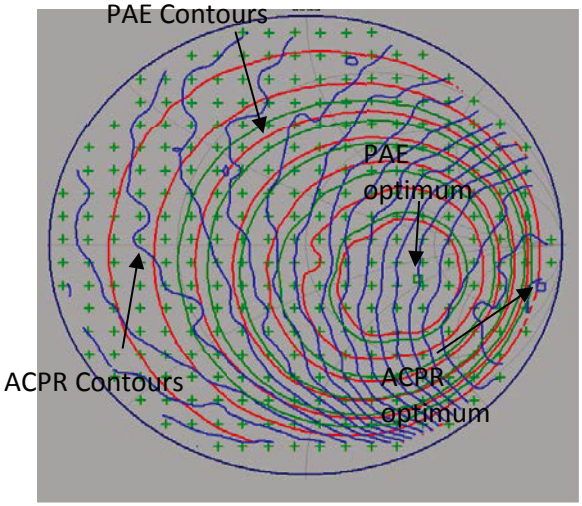

(a)

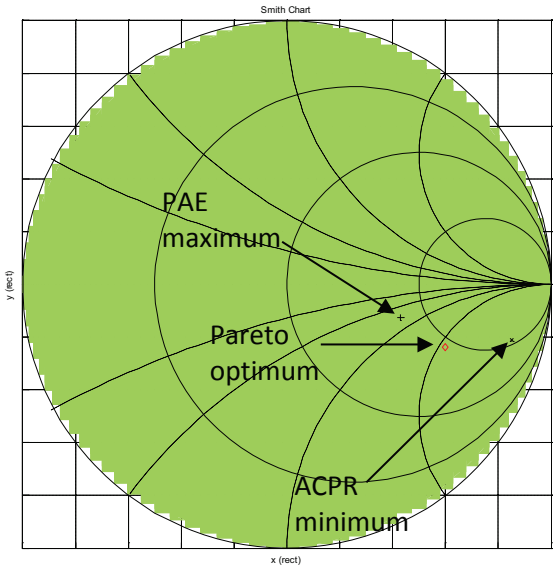

(b)

Fig. 3.10. (a) Traditionally measured load-pull contours for PAE and ACPR with the PAE and ACPR optima indicated, and (b) Pareto optimum as calculated from the traditional load-pull measurement, with the PAE and ACPR optima also indicated

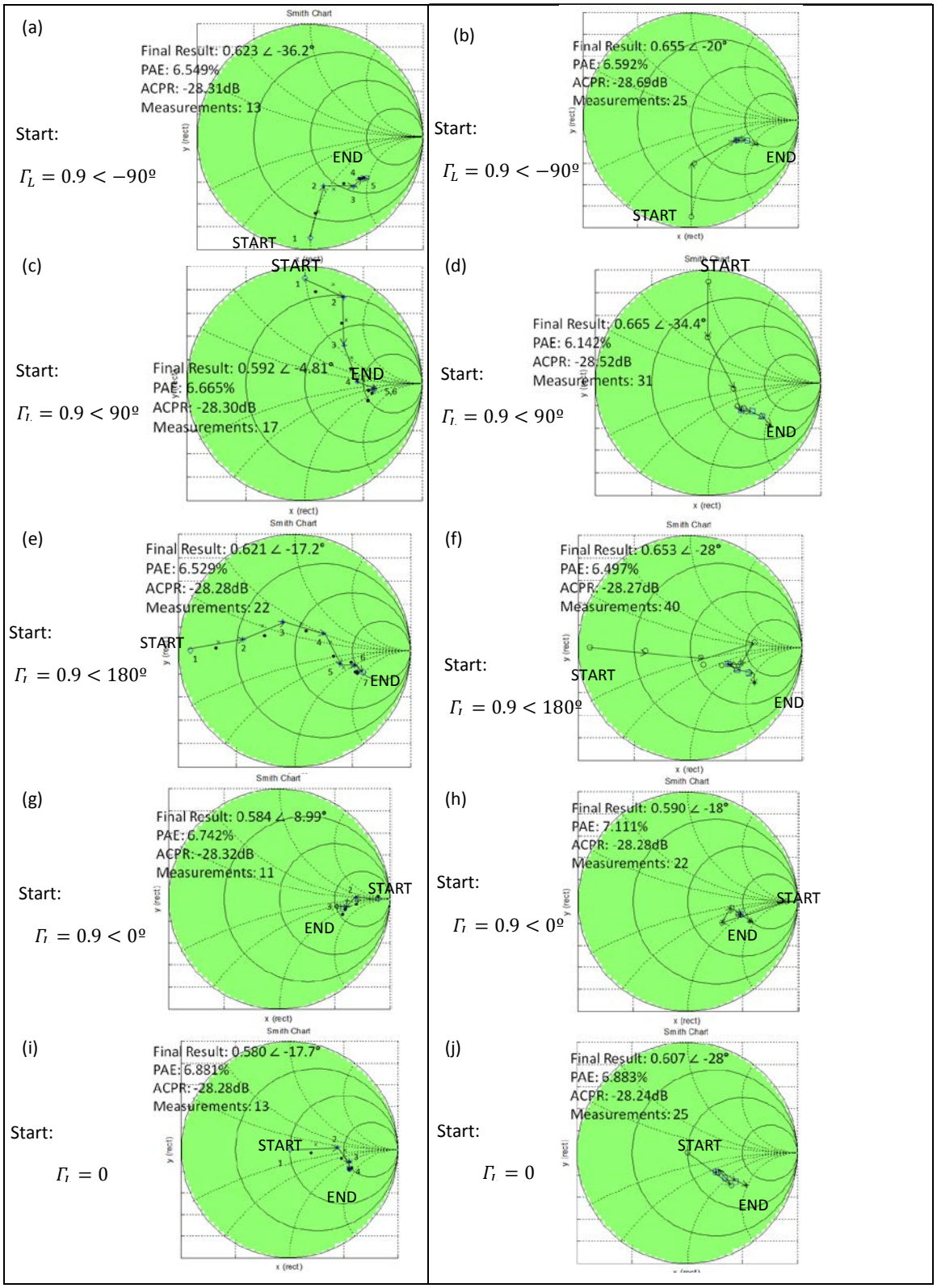

Fig. 3.11. New algorithm measurement search results (left column) and measurement search results for comparison algorithm presented in [4] (right column) from different starting Γ_L values

Table 3.2: New Algorithm Measurement Results

Start Γ_L	End Γ_L	End PAE (%)	End ACPR (dBc)	# Pts.
0.9 <-90º	0.623<-36.2º	6.55	-28.31	13
0.9 <90º	0.592<-4.81º	6.67	-28.30	17
0.9 <180º	0.621<-17.2º	6.53	-28.28	22
0.9<0º	0.584<-8.99º	6.74	-28.32	11
0	0.580<-17.7º	6.88	-28.28	13

Table 3.3: Comparison between algorithms

Start Γ_L	New Algorithm End PAE (%)	Algorithm from [4] End PAE (%)	New Alg'm # Pts.	Alg'm from [4] # Pts.	% Red.
0.9 <-90º	6.55	6.59	13	25	48%
0.9 <90º	6.67	6.14	17	31	45%
0.9 <180º	6.53	6.50	22	40	45%
0.9<0º	6.74	7.11	11	22	50%
0	6.88	6.88	13	25	48%

As in the ADS simulation results, the new algorithm consistently finds results with ACPR less than the limit and with minor variations in PAE. Once again the end locations vary somewhat, but the PAE does not vary enough for that to be a concern. Comparison with the two-step algorithm truly showcases the strength of the new, vector-

based algorithm. The results for both algorithms have similar levels of quality, but the new algorithm consistently finds its optimum result with 45 to 50% fewer measurements. The presented algorithm demonstrates a significant savings in the number of measurements required to optimize the load reflection coefficient for a radar power amplifier.

3.4 Summary

This chapter has presented a direct algorithm for optimization of the load impedance for a radar power amplifier. This algorithms will obtain the highest possible PAE while meeting ACPR requirements. Significant improvement over previous versions of this algorithm has been demonstrated, and the success of the new algorithm has been shown in both simulation and measurement. This work can be broadly applied to both real-time reconfigurable systems and bench-top laboratory measurements.

CHAPTER FOUR

Waveform Optimization using the Ambiguity Function

This chapter published as: [2] Fellows, M.; Baylis, C.; Cohen, L.; Marks, R.J.,"Radar Waveform Optimization to Minimize Spectral Spreading and Achieve Target Detection," *Wireless and Microwave Circuits and Systems (WMCS), 2013 Texas Symposium on* , vol., no., pp.1,4, 4-5 April 2013

The second portion of the real-time radar optimization is the waveform optimization. The proposed method for waveform optimization uses the ambiguity function, which is described in chapter 2. The optimization uses a minimax approach to minimize the ambiguity function at specific coordinates in the ambiguity function, which is ideal for optimizing the radar waveform to detect multiple targets. It also ensures that the optimized waveform meets specified spectral mask requirements. Section 4.1 contains the math which shows how the ambiguity function can be optimized for multiple targets, Section 4.2 shows the optimization process, and Section 4.3 shows computer simulation results for using this process.

4.1 Math behind Waveform Optimization using the Ambiguity Function

In order to show mathematically that minimizing the ambiguity function at target coordinates will improve the waveform's ability to detect a second target at those coordinates, it is necessary to consider both the ambiguity function and the range-Doppler correlation for multiple targets. The range-Doppler correlation is used as a start point for mathematically comparing the received signal from a radar to the transmitted signal. When a radar signal reflects off the target and returns, the return signal should be

a version of the original signal that has been shifted in time depending on the range of the target, and shifted in frequency depending on the radial speed of the target. We define the range-Doppler correlation for a single target as

$$\psi_{R,D}(\tau,u) = \int_{t=-\infty}^{\infty} R(t)T^*(t-\tau)e^{-j2\pi u(t-\tau)}dt \tag{4.1}$$

In (4.1), $R(t)$ is the signal received by a radar, and $T(t)$ is the signal transmitted by the radar. Suppose that instead of the received signal from (4.1) corresponding to a single target, suppose that a signal is received from two targets. This gives a two-target range-Doppler correlation:

$$\psi_{R,D}(\tau,u) = \int_{t=-\infty}^{\infty}[R_1(t)+R_2(t)]T^*(t-\tau)e^{-j2\pi u(t-\tau)}dt. \tag{4.2}$$

Now apply an arbitrary transmitted signal with arbitrary received time delays $(\Delta t_1, \Delta t_2)$, Doppler shifts $(\Delta f_1, \Delta f_2)$, and attenuation factors (a_1, a_2) so that

$$T(t) = s(t) \tag{4.3}$$

$$R_1(t) = a_1 T(t-\Delta t_1)e^{j2\pi\Delta f_1(t-\Delta t_1)} = a_1 s(t-\Delta t_1)e^{j2\pi\Delta f_1(t-\Delta t_1)} \tag{4.4}$$

$$R_2(t) = a_2 T(t-\Delta t_2)e^{j2\pi\Delta f_2(t-\Delta t_2)} = a_2 s(t-\Delta t_2)e^{j2\pi\Delta f_2(t-\Delta t_2)}. \tag{4.5}$$

This leads to the correlation

$$\psi_{R,D}(\tau,u) = \int_{t=-\infty}^{\infty} \begin{matrix}[a_1 s(t-\Delta t_1)e^{j2\pi\Delta f_1(t-\Delta t_1)} + \\ a_2 s(t-\Delta t_2)e^{j2\pi\Delta f_2(t-\Delta t_2)}]s^*(t-\tau)e^{-j2\pi u(t-\tau)}dt\end{matrix}. \tag{4.6}$$

Separating the integrals gives

$$\Psi_{R,D}(\tau,u) = \int_{t=-\infty}^{\infty} a_1 s(t-\Delta t_1)e^{j2\pi\Delta f_1(t-\Delta t_1)}s^*(t-\tau)e^{-j2\pi u(t-\tau)}dt$$

$$+\int_{t=-\infty}^{\infty} s(t-\Delta t_2)e^{j2\pi\Delta f_2(t-\Delta t_2)}]s^*(t-\tau)e^{-j2\pi u(t-\tau)}dt. \quad (4.7)$$

Now expand powers and combine like terms to obtain

$$\Psi_{R,D}(\tau,u) = a_1 e^{j2\pi(u\tau-\Delta f_1\Delta t_1)}\int_{t=-\infty}^{\infty} s(t-\Delta t_1)s^*(t-\tau)e^{j2\pi(\Delta f_1-u)t}dt$$

$$+a_2 e^{j2\pi(u\tau-\Delta f_2\Delta t_2)}\int_{t=-\infty}^{\infty} s(t-\Delta t_2)s^*(t-\tau)e^{j2\pi(\Delta f_2-u)t}dt. \quad (4.8)$$

This is the two target range-Doppler correlation. Now, for time and Doppler shift corresponding to the first target, $\tau = \Delta t_1$ and $u = \Delta f_1$ are applied to get

$$\Psi_{R,D}(\tau,u) = a_1 e^{j2\pi(\Delta f_1\Delta t_1-\Delta f_1\Delta t_1)}\int_{t=-\infty}^{\infty} s(t-\Delta t_1)s^*(t-\Delta t_1)e^{j2\pi(\Delta f_1-\Delta f_1)t}dt$$

$$+a_2 e^{j2\pi(\Delta f_1\Delta t_1-\Delta f_2\Delta t_2)}\int_{t=-\infty}^{\infty} s(t-\Delta t_2)s^*(t-\Delta t_1)e^{j2\pi(\Delta f_2-\Delta f_1)t}dt \quad (4.9)$$

which simplifies to

$$\Psi_{R,D}(\tau,u) = a_1\int_{t=-\infty}^{\infty}|s(t-\Delta t_1)|^2dt$$

$$+a_2 e^{j2\pi(\Delta f_1\Delta t_1-\Delta f_2\Delta t_2)}\int_{t=-\infty}^{\infty} s(t-\Delta t_2)s^*(t-\Delta t_1)e^{j2\pi(\Delta f_2-\Delta f_1)t}dt. \quad (4.10)$$

This result is the energy of the first signal multiplied by its attenuation factor) plus the correlation between the first signal and the second signal. Similarly, apply $\tau = \Delta t_2$ and $u = \Delta f_2$ to (4.8) to obtain

$$\Psi_{R,D}(\tau,u) = a_1 e^{j2\pi(\Delta f_2\Delta t_2-\Delta f_1\Delta t_1)}\int_{t=-\infty}^{\infty} s(t-\Delta t_1)s^*(t-\Delta t_2)e^{j2\pi(\Delta f_1-\Delta f_2)t}dt$$

$$+a_2 e^{j2\pi(\Delta f_2\Delta t_2-\Delta f_2\Delta t_2)}\int_{t=-\infty}^{\infty} s(t-\Delta t_2)s^*(t-\Delta t_2)e^{j2\pi(\Delta f_2-\Delta f_2)t}dt \quad (4.11)$$

which simplifies to

$$\Psi_{R,D}(\tau,u) = a_1 e^{j2\pi(\Delta f_2\Delta t_2-\Delta f_1\Delta t_1)}\int_{t=-\infty}^{\infty} s(t-\Delta t_1)s^*(t-\Delta t_2)e^{j2\pi(\Delta f_1-\Delta f_2)t}dt$$

$$+a_2 \int_{t=-\infty}^{\infty} |s(t-\Delta t_2)|^2 dt \tag{4.12}$$

As in (4.10), this result is the energy of the second signal (divided by its attenuation factor) plus the correlation between the second signal and the first signal. Now we compare to the ambiguity function, which will require centering the range-Doppler correlation for one reflected signal, then doing the same for the other reflected signal. In order to center the correlation for the first reflected signal, apply the following to (4.8):

$$t_1' = t - \Delta t_1 \tag{4.13}$$

$$dt_1' = dt \tag{4.14}$$

$$\tau_1' = \tau - \Delta t_1 \tag{4.15}$$

$$u_1' = u - \Delta f_1. \tag{4.16}$$

This gives

$$\chi(\tau_1', u_1')$$

$$= a_1 e^{j2\pi\begin{pmatrix}(u_1'+\Delta f_1)(\tau_1'+\Delta t_1)\\ -\Delta f_1 \Delta t_1\end{pmatrix}} \int_{t=-\infty}^{\infty} s\begin{pmatrix}(t_1'+\Delta t_1)\\ -\Delta t_1\end{pmatrix} s^*\begin{pmatrix}(t_1'+\Delta t_1)-\\ (\tau_1'+\Delta t_1)\end{pmatrix} e^{j2\pi\begin{pmatrix}\Delta f_1-(u_1')\\ +\Delta f_1)\end{pmatrix}(t_1'+\Delta t_1)} dt_1'$$

$$+a_2 e^{j2\pi\begin{pmatrix}(u_1'+\Delta f_1)(\tau_1'+\Delta t_1)\\ -\Delta f_2 \Delta t_2\end{pmatrix}} \int_{t=-\infty}^{\infty} s\begin{pmatrix}(t_1'+\Delta t_1)\\ -\Delta t_2\end{pmatrix} s^*\begin{pmatrix}(t_1'+\Delta t_1)-\\ (\tau_1'+\Delta t_1)\end{pmatrix} e^{j2\pi\begin{pmatrix}\Delta f_2\\ -(u_1'+\Delta f_1)\end{pmatrix}(t_1'+\Delta t_1)} dt_1' \tag{4.17}$$

Expand powers and combine like terms to obtain

$\chi(\tau_1', u_1') =$

$a_1 e^{j2\pi(u_1'\tau_1' + \tau_1'\Delta f_1 + u_1'\Delta t_1)} \int_{t=-\infty}^{\infty} s(t_1') s^*(t_1' - \tau_1') e^{-j2\pi(u_1' t_1' + u_1'\Delta t_1)} dt_1' +$

$a_2 e^{j2\pi(u_1'\tau_1' + \tau_1'\Delta f_1 - \Delta f_2\Delta t_2 + u_1'\Delta t_1 + \Delta f_1\Delta t_1)}$

$$\int_{t=-\infty}^{\infty} s(t_1' + \Delta t_1 - \Delta t_2) s^*(t_1' - \tau_1') e^{j2\pi(\Delta f_2 t_1' + \Delta f_2\Delta t_1 - u_1' t_1' - u_1'\Delta t_1 - \Delta f_1 t_1' - \Delta f_1\Delta t_1)} dt_1' \tag{4.18}$$

and simplify to

$$\chi(\tau_1', u_1') = a_1 e^{j2\pi\tau_1'(u_1' + \Delta f_1)} \int_{t=-\infty}^{\infty} s(t_1') s^*(t_1' - \tau_1') e^{-j2\pi u_1' t_1'} dt_1'$$

$$+ a_2 e^{j2\pi\begin{pmatrix} u_1'\tau_1' + \tau_1'\Delta f_1 \\ +\Delta f_2\Delta t_1 - \Delta f_2\Delta t_2 \end{pmatrix}} \int_{t=-\infty}^{\infty} s\begin{pmatrix} t_1' + \Delta t_1 \\ -\Delta t_2 \end{pmatrix} s^*(t_1' - \tau_1') e^{j2\pi\begin{pmatrix} \Delta f_2 t_1' \\ -u_1' t_1' - \Delta f_1 t_1' \end{pmatrix}} dt_1'. \tag{4.19}$$

Note that this output from the correlator is equal to the single target ambiguity function (2.2) for the first reflected signal plus some extra terms caused by the second target. Now take (4.8) and center it for the signal reflected from the second target by applying

$$t_2' = t - \Delta t_2 \tag{4.20}$$

$$dt_2' = dt \tag{4.21}$$

$$\tau_2' = \tau - \Delta t_2 \tag{4.22}$$

$$u_2' = u - \Delta f_2. \tag{4.23}$$

This leads to

$\chi(\tau_2', u_2') =$

$$a_1 e^{j2\pi\begin{pmatrix} (u_2' + \Delta f_2)(\tau_2' + \Delta t_2) \\ -\Delta f_1\Delta t_1 \end{pmatrix}} \int_{t=-\infty}^{\infty} s\begin{pmatrix} (t_2' + \Delta t_2) \\ -\Delta t_1 \end{pmatrix} s^*\begin{pmatrix} (t_2' + \Delta t_2) \\ - \\ (\tau_2' + \Delta t_2) \end{pmatrix} e^{j2\pi\begin{pmatrix} \Delta f_1 \\ -(u_2' + \Delta f_2) \end{pmatrix}(t_2' + \Delta t_2)} dt_2'$$

$$+a_2 e^{j2\pi\binom{(u_2'+\Delta f_2)(\tau_2'+\Delta t_2)}{-\Delta f_2 \Delta t_2}} \int_{t=-\infty}^{\infty} s\binom{(t_2'+\Delta t_2)}{-\Delta t_2} s^*\binom{(t_2'+\Delta t_2)-}{(\tau_2'+\Delta t_2)} e^{j2\pi\binom{\Delta f_2}{-(u_2'+\Delta f_2)}(t_2'+\Delta t_2)} dt_2' \tag{4.24}$$

Expand powers and combine like terms to obtain

$$\begin{aligned}
&\chi(\tau_2', u_2') \\
&= a_1 e^{j2\pi(u_2'\tau_2'+\tau_2'\Delta f_2+u_2'\Delta t_2+\Delta f_2\Delta t_2-\Delta f_1\Delta t_1)} \\
&\cdot \int_{t=-\infty}^{\infty} s\binom{t_2'+\Delta t_2}{-\Delta t_1} s^*(t_2'-\tau_2') e^{j2\pi(\Delta f_1 t_2'+\Delta f_1\Delta t_2-u_2't_2'-u_2'\Delta t_2-\Delta f_2 t_2'-\Delta f_2\Delta t_2)} dt_2' \\
&\quad +a_2 e^{j2\pi(u_2'\tau_2'+\tau_2'\Delta f_2+u_2'\Delta t_2)} \int_{t=-\infty}^{\infty} s(t_2') s^*(t_2'-\tau_2') e^{-j2\pi(u_2't_2'+u_2'\Delta t_2)} dt_2'
\end{aligned} \tag{4.25}$$

and simplify to

$$\begin{aligned}
\chi(\tau_2', u_2') &= a_1 e^{j2\pi\binom{u_2'\tau_2'+\tau_2'\Delta f_2}{+\Delta f_1\Delta t_2-\Delta f_1\Delta t_1}} \int_{t=-\infty}^{\infty} s\binom{t_2'+\Delta t_2}{-\Delta t_1} s^*(t_2'-\tau_2') e^{j2\pi\binom{\Delta f_1 t_2'-u_2't_2'}{-\Delta f_2 t_2'}} dt_2' \\
&\quad +a_2 e^{j2\pi\tau_2'(u_2'+\Delta f_2)} \int_{t=-\infty}^{\infty} s(t_2') s^*(t_2'-\tau_2') e^{-j2\pi u_2't_2'} dt_2'.
\end{aligned} \tag{4.26}$$

This output from the correlator is equal to the single target ambiguity function for the second reflected signal plus some extra terms caused by the first reflected signal. The extra terms in (4.26) are very similar to the extra terms in (4.19). In fact, simply swapping out all the subscripts (ie. t_1' becomes t_2') will change (4.19) to (4.26). This shows the symmetry of the function and should mean that minimizing a location on the first reflected signal's ambiguity function that corresponds to the range and Doppler shift of the second reflected signal should also succeed in minimizing a location on the second reflected signal's ambiguity function that corresponds to the range and Doppler shift of the first target.

4.2 Process for Waveform Optimization using the Ambiguity Function

As shown in the previous section, the waveform can be optimized for distinguishing between targets by minimizing the ambiguity function at the coordinates of secondary targets. This chapter details a method for this optimization in which the user specifies an arbitrary number of minimization points, and the algorithm chooses the ideal waveform for those minimization points from a predefined library of waveforms. First, the algorithm compares the simulated spectrum for each waveform to a spectral mask and eliminates any waveforms that do not pass the mask. The algorithm then uses a *minimax* method to find the best one for the specified minimization points. Specifically, the *minimax* method finds the maximum value of the ambiguity function at the designated minimization points (the *minimax* value) for each passing waveform, and then ranks the waveforms from the smallest *minimax* value (best) to the largest *minimax* value (worst). For results using only computer simulations, the best waveform from these rankings is automatically chosen as the optimum. However, an extra step can be added to insure that waveform will also pass the spectral mask after being amplifier. For that step, the waveforms are implemented from best to worst on the test bench mentioned in chapter 3, and the first one to pass the spectral mask in the test bench measurement is chosen as the optimum waveform.

4.3 Optimization Results

This search approach was tested for optimization over a library of linear frequency-modulated (FM) chirp waveforms. For the tests shown below, the library of waveforms was made up of linear frequency-modulated chirps with constant pulse duration and bandwidths varying from a 5 MHz up-chirp to a 5 MHz down chirp in steps

of 250 kHz. As mentioned in Chapter 2, the chirp waveform gives an ambiguity function with a triangle shape that can be rotated, according to the ratio of the pulse width to the bandwidth of the chirp [32]. Figures 4 and 5 show two results for using this algorithm in computer simulation. In each figure, (a) is the ambiguity function for the chosen chirp (with the minimization points shown by the yellow arrows), (b) shows the frequency vs time characteristic of the chosen chirp, and (c) shows the spectrum vs the spectral mask for the chosen chirp.

As each result shows, the chirp's ambiguity function is rotated such that the magnitude of the ambiguity function at the minimization points remains low. The result in figure 4.1 is a 1.75 MHz down chirp, which just barely passes the spectral mask. The minimization points in Figure 4.1(a) give a result that would be good for a range-focused radar. The result in figure 4.2 is a 500 kHz up chirp. This chirp passes the spectral mask quite easily, which makes sense from the narrower bandwidth. The minimization points in figure 4.2(a) result in a more Doppler-focused radar waveform.

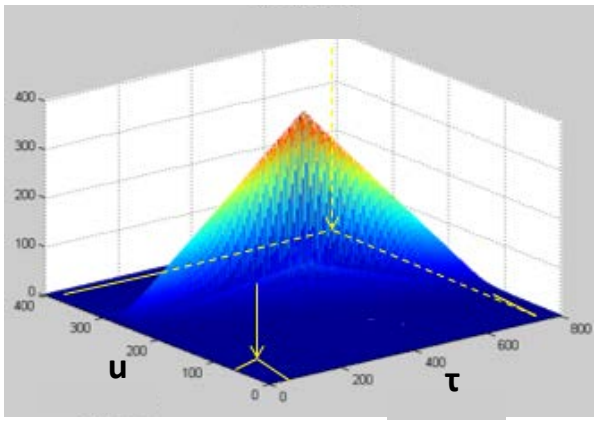

(a)

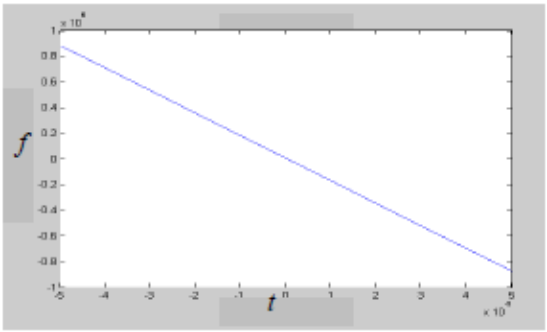

(b)

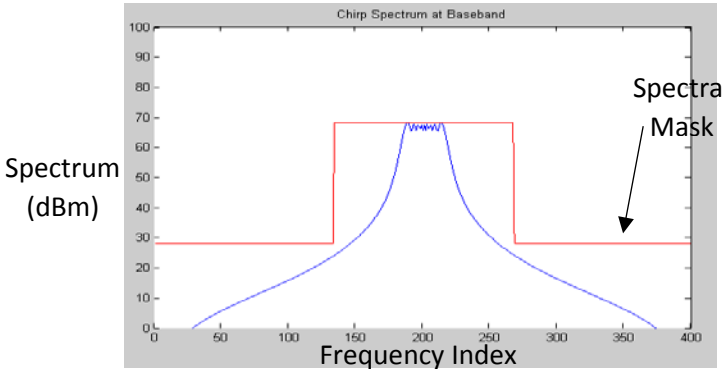

(c)

Fig. 4.1. (a) Ambiguity function magnitude with arrows representing range-Doppler combinations selected for minimization, (b) frequency vs time plot, and (c) baseband spectrum and spectral mask for the best chirp

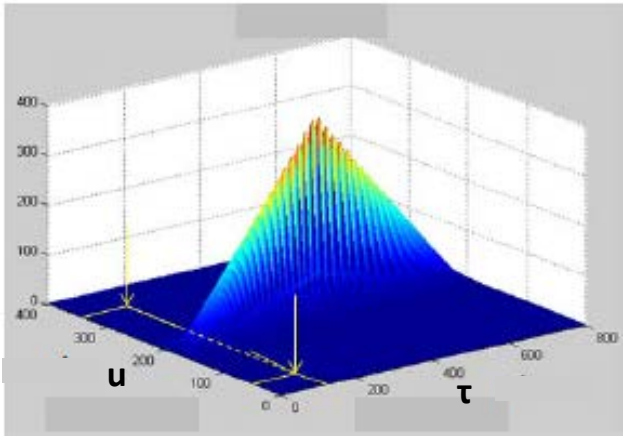

(a)

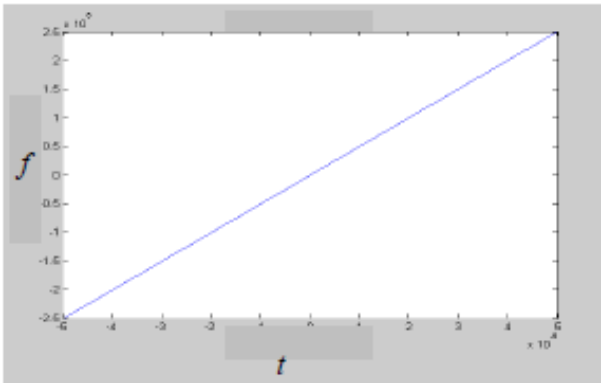

(b)

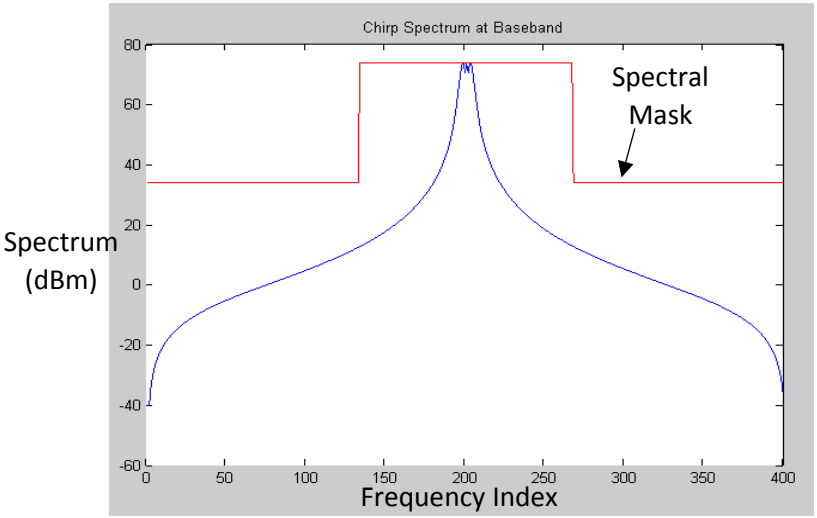

(c)

Fig. 4.2. (a) Ambiguity function magnitude with arrows representing range-Doppler combinations selected for minimization, (b) frequency vs time plot, and (c) baseband spectrum and spectral mask for the best chirp

Figure 4.3 shows the result for implementing the test bench portion of the algorithm in addition to the computer simulation portion. As mentioned previously, the only difference between the simulation-only version of the optimization and this version is that this version contains a measurement of the spectrum at the output of a radar amplifier, in order to confirm that the spectrum still passes the mask. For Figure 4.3, the minimization points are indicated by the red arrows. Figure 4 contains the same parts as the previous two figures. Figure 4.4 shows the result when the waveform is passed through an amplifier and measured with a spectrum analyzer. The chirp implemented on the test bench has a center frequency of 3.3 GHz, which can be seen in the spectrum analyzer measurement of figure 4.4.

Again, this result shows a low magnitude for the ambiguity function at the minimization points. Like in figure 4.1, this the minimization locations for this result gives a chirp with 1.75 MHz bandwidth. The results shown in figures 4.1, 4.2, and 4.3 show that the waveform optimization using the ambiguity function effectively chooses a radar waveform for an adaptive radar system.

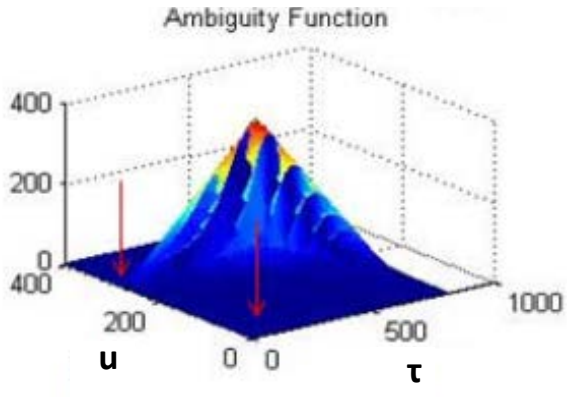

(a)

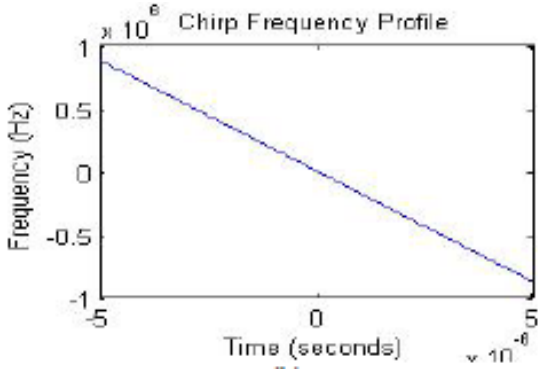

(b)

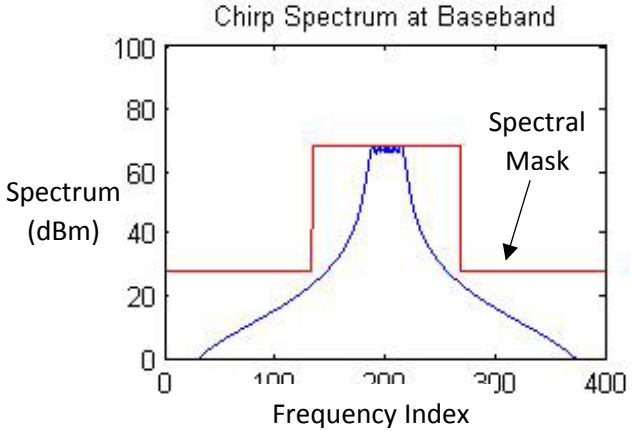

(c)

Fig. 4.3. (a) Ambiguity function magnitude, (b) frequency vs time plot, and (c) baseband spectrum and spectral mask for the best chirp

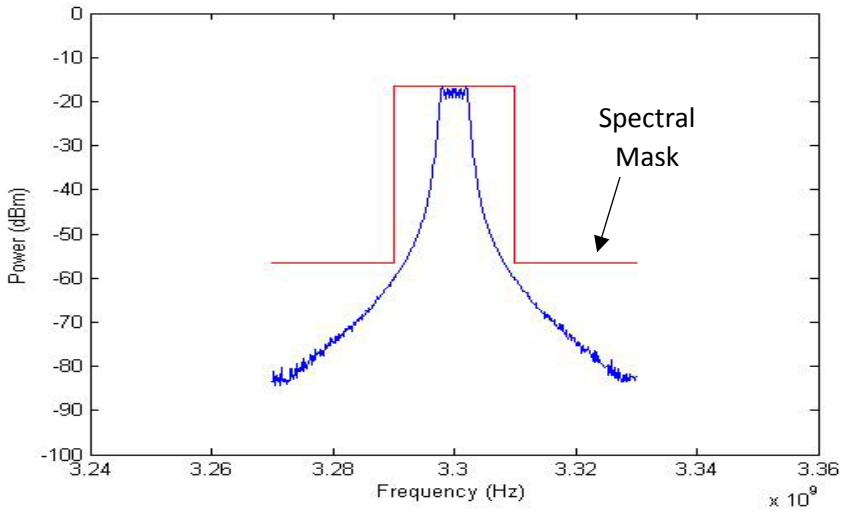

Fig. 4.4. Spectrum analyzer measured spectrum and spectral mask

4.4 Summary

This chapter has discussed a waveform optimization using the ambiguity function. This optimization will choose the best spectrally compliant waveform for detection of targets at various minimization locations using the ambiguity function. Several results have been shown proving the success of the *minimax* approach used to choose the spectrally compliant waveform with the best ambiguity function out of the provided library. This technique has been shown to work in computer simulation, with the ability to check if the chosen waveform will still pass a spectral mask after being amplifier and measured on a spectrum analyzer.

CHAPTER FIVE

Conclusion

This thesis has presented an algorithm for optimizing the load impedance for a radar power amplifier and an algorithm for choosing a good chirp waveform for target detection and spectral compliance. The key contribution of both algorithms is that they are sensitive to concerns of spectral compliance. The circuit optimization has been shown to improve significantly on the number of measurements required to perform such an optimization. It should be noted, however, that the circuit optimization does still have two potential weaknesses. First, the circuit optimization will not handle encounters with local minima in ACPR or local maxima in PAE. Such measurements would result in a false Pareto front, which could lead to a less ideal result. Second, the fact that the presented version of the circuit optimization uses ACPR for its limit means that it does not account for a spectral mask that is not flat in the out-of-band regions. Real spectral masks are often sloped downward in the out-of-band regions. This allows more spectral spreading close to the operating channel, but requires that power levels be lower at frequencies further from the operating channel. The waveform optimization does not have any obvious weaknesses such as those, but it also does not employ any intelligent search techniques to make the problem easier. It searches through the entire library of waveforms it is given and finds the result using a brute force approach.

In ongoing and future work, it is expected that new and better versions of these algorithms will be presented. In the area of circuit optimization, a new measure of spectral compliance is being developed that allows circuit optimization based directly on

spectral mask compliance instead of ACPR. In addition, other search techniques may be tested in order to assure that the ideal type of search is being implemented. In the area of waveform optimization, the idea of using machine intelligent search techniques is also being considered.

The big picture in the future of these optimizations, however, is a joint optimization that will combine elements from both the waveform and the circuit optimizations to create new optimizations. The new optimizations will seek to find the best waveform and circuit simultaneously. This is a necessary and useful step for cognitive radar because the variables will be interdependent on each other. The ambiguity function will be affected by the load impedance at the output of the power amplifier, and the best circuit to choose will be dependent on the bandwidth of the signal used. Future optimizations to jointly optimize waveform and circuit would likely operate in a three-dimensional search space, varying waveform/bandwidth and load reflection coefficient simultaneously. The optimizations presented in this thesis are a good step toward a spectrally sensitive cognitive radar system. Combining the two optimizations into one is expected to make the optimization process even faster and more effective.

BIBLIOGRAPHY

[1] Fellows, M.; Baylis, C.; Martin, J.; Cohen, L.; Marks, R.J., "Direct Algorithm for the Pareto Load-Pull Optimization of Power-Added Efficiency and Adjacent-Channel Power Ratio," –accepted for publication by IET Radar, Sonar, and Navigation.

[2] Fellows, M.; Baylis, C.; Cohen, L.; Marks, R.J., "Radar Waveform Optimization to Minimize Spectral Spreading and Achieve Target Detection," *Wireless and Microwave Circuits and Systems (WMCS), 2013 Texas Symposium on* , vol., no., pp.1,4, 4-5 April 2013

[3] J. de Graaf, H. Faust, J. Alatishe, and S. Talapatra, "Generation of Spectrally Confined Transmitted Radar Waveforms," Proceedings of the IEEE Conference on Radar, 2006, pp. 76-83

[4] J. Martin, *Adaptive Load Impedance Optimization for Power Amplifiers in Reconfigurable Radar Transmitters*, Master's Thesis, Baylor University, 2012.

[5] Y. Collette and P. Siarry, *Multiobjective Optimization: Principles and Case Studies*, Springer, 2004.

[6] H.C. Calpine and A. Golding, "Some Properties of Pareto-Optimal Choices in Decision Problems," *Omega* 4, No. 2 (1976): 141-147.

[7] T. Getachew, M. Kostreva, and L. Lancaster. "A Generalization of Dynamic Programming for Pareto Optimization in Dynamic Networks." *RAIRO-Operations Research* 34.1 (2000): 27-47.

[8] R.T. Marler and J.S. Arora. "Survey of Multi-Objective Optimization Methods for Engineering." *Structural and Multidisciplinary Optimization* 26.6 (2004): 369-395.

[9] K. Deb, "Multi-Objective Optimization." *Search Methodologies*, Springer U.S., 2005. 273-316.

[10] I. Das and J. E. Dennis, "Normal-Boundary Intersection: A New Method for Generating the Pareto Surface in Nonlinear Multicriteria Optimization Problems," *SIAM J. on Optimization*, 631-657, March 1998.

[11] I.Y.Kim and O. de Weck, "Adaptive Weighted Sum Method for Multiobjective Optimization: A New Method for Pareto Front Generation", *Structural and Multidisciplinary Optimization*, Vol. 31, pp. 105-116, 2006.

[12] J. Sevic, K. Burger, and M. Steer, "A Novel Envelope-Termination Load-Pull Method for ACPR Optimization of RF/Microwave Power Amplifiers," 1998 IEEE MTT-S International Microwave Symposium Digest, June 1998, Vol. 2, pp. 723-726.

[13] F. Raab, P. Asbeck, S. Cripps, P. Kenington, Z. Popovic, N. Pothecary, J. Sevic, and N. Sokal, "RF and Microwave Power Amplifier and Transmitter Topologies, Part 1," *High Frequency Electronics*, May 2003.

[14] International Telecommunication Union Standard ITU-R SM.1541, "Unwanted Emissions in the Out-of-Band Domain."

[15] C. Baylis, L. Wang, M. Moldovan, J. Martin, H. Miller, L. Cohen, and J. de Graaf, "Designing Transmitters for Spectral Conformity: Power Amplifier Design Issues and Strategies," *IET Radar, Sonar & Navigation*, Vol. 5, No. 6, July 2011, pp. 681-685.

[16] C. Baylis, L. Wang, M. Moldovan, J. Martin, H. Miller, L. Cohen, and J. de Graaf, "Designing for Spectral Conformity: Issues in Power Amplifier Design," Waveform Diversity and Design Conference, Niagara Falls, Ontario, Canada, August 2010.

[17] J. Sevic, "Large Signal Automated Load-Pull Characterization of Adjacent-Channel Power Ratio for Digital Wireless Communication Systems," 1996 IEEE MTT-S International Microwave Symposium Digest, June 1996, pp. 763-766.

[18] Q. Wu, H. Xiao, and F. Li, "Linear Power Amplifier Design for CDMA Signals: A Spectrum Analysis Approach," *Microwave Journal*, 1998.

[19] Y Sun, "Evolutionary Tuning Method for Automatic Impedance Matching in Communication Systems," Proceedings of the 1998 IEEE International Conference on Electronics, Circuits, and Systems, Vol. 3, pp. 73-77.

[20] Y. Sun and W.K. Lau, "Antenna Impedance Matching Using Genetic Algorithms," Proceedings of the IEE Conference on Antennas and Propagation, York, United Kingdom, August 1999, pp. 31-36.

[21] D. Qiao, R. Molfino, S. Lardizabal, B. Pillans, P. Asbeck, and G. Jerinic, "An Intellwigently Controlled RF Power Amplifier with a Reconfigurable MEMS-Varactor Tuner," *IEEE Transactions on Microwave Theory and Techniques*, Vol. 53, No. 3, Part 2, March 2005, pp. 1089-1095.

[22] W. du Plessis and P. Abrie, "Lumped Impedance Matching Using a Hybrid Genetic Algorithm," *Microwave and Optical Technology Letters*, Vol. 37, No. 3, pp. 201-212, May 2003.

[23] E. Arroyo-Huerta, A. Diaz-Mendez, J. Ramirez Cortes, and J. Garcia, "An Adaptive Impedance Matching Approach Based on Fuzzy Control," 52nd IEEE International Midwest Symposium on Circuits and Systems, August 2009, pp. 889-892.

[24] J. Hemminger, "Antenna Impedance Matching With Neural Networks," *International Journal of Nerual Systems* (IJNS), Vol. 15, No. 5, pp. 357-361, 2005.

[25] A. Mushi, D. Johns, and A. Sedra, "Adaptive Impedance Matching," Proceedings of the IEEE International Symposium on Circuits and Systems, 1994 (ISCAS '94), Vol. 2, pp. 69-72.

[26] C. Baylis, L. Dunleavy, S. Lardizabal, R.J. Marks II, and A. Rodriguez, "Efficient Optimization Using Experimental Queries; A Peak-Search Algorithm for Efficient Load-Pull Measurements," *Journal of Advanced Computational Intelligence and Intelligent Informatics*, Vol. 15, No. 1, January 2011.

[27] J. Martin, M. Moldovan, C. Baylis, R.J. Marks II, L. Cohen, and J. de Graaf, "Radar Chirp Waveform Selection and Circuit Optimization Using ACPR Load-Pull Measurements," 2012 IEEE Wireless and Microwave Technology Conference (WAMICON 2012), Cocoa Beach, Florida, April 2012.

[28] R. Chen and B. Cantrell, "Highly Bandlimited Radar Signals,"Proceedings of the 2002 IEEE Radar Conference, pp. 220-226.

[29] S. Blunt, M. Cook, E. Perrins, and J. de Graaf, "CPM-Based RadarWaveforms for Efficiently Bandlimiting a Transmitted Spectrum," 2009 IEEE Radar Conference, pp. 1-6.

[30] M. Cook, M.S. Thesis: *CPM-Based Radar Waveforms for EfficientlyBandlimiting a Transmitted Spectrum*, University of Kansas, April 2010.

[31] M. Moldovan, C. Baylis, R.J. Marks II, L. Cohen, and J. de Graaf,"Radar Chirp Waveform Selection and Circuit Optimization Using ACPR Load-Pull Measurements," IEEE Wireless and Microwave Technology Conference, Cocoa Beach, Florida, April 2012.

[32] M. Skolnik, *Introduction to Radar Systems*, Third Edition, McGraw-Hill, 2001.

[33] L. Patton, *On the Satisfaction of Modulus and Ambiguity Function Constraints in Radar Waveform Optimization for Detection*, Doctoral Disseration, Wright State University, 2007.

[34] J. Holtzman and J. Thorp, "Optimum Signals for Radar," *IEEE Transactions on Aerospace and Electronic Systems,* Vol. 5, No. 6, pp.898-905, November 1969.

[35] K. Wong and W.-K. Chung, "Pulse-Diverse Radar/Sonar FSK-PSK Waveform Design to Emphasize/De-Emphasize Designated Doppler-Delay Sectors," IEEE Radar Conference, Alexandria, Virginia, May 2000, pp. 745-749.

[36] S. Sussman, "Least-Square Synthesis of Radar Ambiguity Functions," *IRE Transactions on Information Theory*, Vol. 8, No. 3, pp. 246-254, April 1962.

[37] C. Baylis, J. Martin, M. Moldovan, O. Akinbule, and R.J. Marks II, "A Test Platform for Real-Time Waveform and Impedance Optimization in Microwave Radar Systems," 2012 Waveform Diversity and Design Conference, Kauai, Hawaii, January 2012.

[38] Guerci, Joseph R. "Cognitive radar: a knowledge-aided fully adaptive approach." *Radar Conference, 2010 IEEE*. IEEE, 2010.